Sound Source Reconstruction Using Inverse Boundary Element Calculations

Andreas Schuhmacher and Jørgen Hald
Brüel & Kjær A/S, Skodsborgvej 307, DK-2850 Nærum, Denmark

Karsten Bo Rasmussen[a)]
Ørsted•DTU, Section of Acoustic Technology, Building 352, Technical University of Denmark, DK-2800 Kgs. Lyngby, Denmark

Per Christian Hansen
Informatics and Mathematical Modelling, Building 321, Technical University of Denmark, DK-2800 Kgs. Lyngby, Denmark

ABSTRACT

Whereas standard boundary element calculations focus on the forward problem of computing the radiated acoustic field from a vibrating structure, the aim of the present work is to reverse the process, i.e., to determine vibration from acoustic field data. This inverse problem is brought on a form suited for solution by means of an inverse boundary element method. Since the numerical treatment of the inverse source reconstruction results in a discrete ill-posed problem, regularisation is imposed to avoid unstable solutions dominated by errors. In the present work the emphasis is on Tikhonov regularisation and parameter-choice methods not requiring an error norm estimate for choosing the right amount of regularisation. We demonstrate that the L-curve criterion is robust with respect to the errors in real measurement situations.

PACS numbers: 43.20.Fn, 43.35.Sx, 43.60.Cg, 43.60.Sx

[a)] Present address: Oticon A/S, Strandvejen 58, DK-2900 Hellerup, Denmark

INTRODUCTION

The objective of this work is to compute the unknown surface velocity distribution on a complex acoustic source from measured acoustic field data. Hence, we are faced with an inverse source problem to be solved, which involves forming a transfer matrix relating the pressure at every field point to the normal component of the surface velocity[1]. In the present work this forward modelling is done by means of a boundary element method (BEM). So far, direct BEM formulations have been used in most work[2-4], while we have chosen to explore an indirect BEM formulation.

The inverse problem is ill-posed and therefore very sensitive to noise and errors in the measured data. In experimental data a certain amount of errors and contaminating noise are inevitable. In addition, some information about the sound source is lost in the radiation process, and the search for this information simply does not make sense. Hence, when real physical systems are dealt with the challenge is to solve an inverse problem where part of the information is lost. Since the inverse problem is ill posed the transfer matrix computed by the BEM is ill conditioned, thus requiring special treatment. In that respect, the singular value decomposition (SVD) seems to be the preferred tool towards regularising the ill-posed problem. However, no clear guidelines regarding the filtering of the SVD-components have yet been provided.

This work describes an approach to the inverse problem based upon an indirect BEM formulation in conjunction with Tikhonov regularisation, and using the SVD as an analysis tool. The influence of the regularisation parameter and the filtering process associated with Tikhonov regularisation is investigated by means of the L-curve, which is a log-log plot of the solution's norm versus the norm of the residual vector. The L-curve is also used to determine the optimal amount of regularisation, and this method is compared to a similar method: the generalised cross-validation (GCV) technique. A practical case using a car tyre demonstrates the capabilities of our regularisation scheme. In addition, a comparison with near-field acoustic holography is made.

I. BOUNDARY INTEGRAL FORMULATIONS OF THE FORWARD PROBLEM

We consider an exterior acoustic forward problem, that is, only the fluid outside a vibrating source surface is addressed. No secondary sound sources or obstacles exist in the exterior region. In the fluid, the acoustic pressure p must satisfy the Helmholtz equation

$$\nabla^2 p + k^2 p = 0, \tag{1}$$

where k is the acoustic wave number.

Combining this equation with a Neumann boundary condition for the surface S, we can solve the acoustic radiation problem and extract admissible wave functions in the exterior region Ω^+. In addition, the Sommerfeld radiation condition must be satisfied in the exterior region, ensuring that only outgoing waves are considered, i.e.,

$$\lim_{R\to\infty}\left[R\left(\frac{\partial p}{\partial R} + jkp \right)\right] = 0, \tag{2}$$

in which R is the distance from the surface. Hence, we consider the exterior problem

$$\begin{cases} \nabla^2 p + k^2 p = 0 \quad , \quad \text{in } \Omega^+ \\ \text{boundary condition} \quad , \quad \text{on } S, \\ \text{SRC} \end{cases} \tag{3}$$

where SRC denotes the Sommerfeld radiation condition Eq. (2). The problem geometry is shown in Fig.1.

Boundary integral equations provide a complete formulation of the acoustic problem Eq. (3), thus making these equations an obvious choice in connection with radiation and/or scattering problems involving arbitrarily shaped structures. Moreover, they have the advantage that the infinite nature of the exterior region is implicit in the surface representation. The formulations are often classified as either direct or indirect – where the direct formulation corresponds to Helmholtz integral equation and the numerous indirect formulations are based on layer potentials. Below we survey the direct and indirect formulations, and we show how a boundary integral equation in combination with a variational problem can lead to a complete description of the forward acoustic problem. Implementation issues are discussed in Section III.

A. Direct formulation

The direct formulation can be derived from the Helmholtz equation using Green's theorem. Therefore, the integral equation is also known as the Helmholtz integral equation:

$$C(P)\,p(P) = \int_S \left(p(Q)\frac{\partial G(P,Q)}{\partial n_Q} + j\omega\rho\, v_n(Q) G(P,Q) \right) dS(Q) \quad , \quad C(P) = \begin{cases} 1 & , P \text{ in } \Omega^+ \\ \tfrac{1}{2} & , P \text{ on } S \\ 0 & , P \text{ in } \Omega^- \end{cases} \tag{4}$$

Here ω is the angular frequency, ρ is the fluid density, v_n is the normal surface velocity, and $G(P,Q)$ is the free-space Green's function for the Helmholtz equation satisfying the Sommerfeld radiation condition. In 3-D acoustics, Green's function is

$$G(P,Q) = \frac{e^{-jkR}}{4\pi R} \quad , \quad R = |P - Q| \, . \tag{5}$$

The points P and Q are shown in Fig.1 and we can interpret Eq. (5) as an expression for the pressure at point P from a unit point source (monopole) at Q.

A serious shortcoming of the Helmholtz integral Eq. (4) is the failure when it is applied to bodies of thin shape or regular bodies with thin appendages. This thin-shape breakdown of the direct formulation was investigated extensively by Martinez[5] and recently by Cutanda et al.[6], and remedies ensuring a meaningful formulation for thin shapes were proposed.

B. Indirect formulations

In this section we survey four indirect formulations, where the exterior acoustic field is expressed in terms of single-layers, double-layers, or combined single- and double-layers[7] on the source boundary S. Some of the first boundary integral methods to appear were based on a distribution of single-layers on the surface in order to represent the acoustic field[8,9].

For a point P lying strictly in the exterior region, we can express the pressure p_f by the single-layer formulation

$$p_f(P) = -\int_S \sigma(Q)\, G(P,Q)\, dS(Q) \, , \tag{6}$$

where $-\sigma(Q)$ is the unknown source strength at Q on S and subscript f denotes a field quantity. We recognise Green's function in the integrand, and we can view this formulation as a distribution of simple sources (monopoles) on the surface S. Since this representation satisfies the Helmholtz equation and the *SRC* condition, the only remaining issue when solving the exterior Neumann problem is to determine the unknown source strengths $\sigma(Q)$ by matching them to the prescribed normal surface velocity v_n. While the surface pressure is a continuous function across S, the surface velocity v_n exhibits a jump property and thus we can write the unknown source densities σ for Q on S as[10]

$$\sigma(Q) = -j\omega\rho\left(v_n^+(Q) - v_n^-(Q)\right). \tag{7}$$

Once the source strengths $\sigma(Q)$ are known, we are able to find the pressure on the surface or in the exterior by means of surface integration.

Another possibility is to express the field pressure by a double-layer formulation

$$p_f(P) = \int_S \mu(Q)\frac{\partial G(P,Q)}{\partial n_Q} dS(Q), \tag{8}$$

where $\mu(Q)$ is the unknown source density. Such a representation of the exterior field can be viewed as a distribution of double sources (dipoles) over S. A double-layer representation gives rise to a pressure jump across S with a continuous surface velocity, and the unknown density function μ is written for P on S as[10]

$$\mu(Q) = p_s^+(Q) - p_s^-(Q). \tag{9}$$

where $p_s^+(Q)$ and $p_s^-(Q)$ are the pressures on the two sides of the surface at the point Q.

A third alternative is to make use of a combined approach by mixing the two layers and end up with a mixed-layer formulation[7,11]

$$p_f(P) = \int_S \left(G(P,Q) + \alpha\frac{\partial G(P,Q)}{\partial n_Q}\right) h(Q)\, dS(Q). \tag{10}$$

Here $h(Q)$ denotes the source density and α is a complex coupling constant that must be chosen carefully. Provided that $\mathrm{Im}(\alpha) \neq 0$, one can prove that the homogeneous counterpart of Eq. (10) has the trivial solution only[12]. An application of this formulation is provided by Sayhi et al.[11] with a

coupling constant equal to j. The mixed layer formulation is attractive because it can overcome the serious difficulty associated with irregular frequencies, where the equations fail to provide correct and meaningful results. A drawback of the mixed-layer formulation is that the source density $h(Q)$ on S cannot easily be related to the physical variables pressure and normal surface velocity.

As yet an alternative formulation we can combine Eqs. (6) and (8) to obtain what is known as a jump formulation,

$$p_f(P) = \int_S \left(-\sigma(Q)G(P,Q) + \mu(Q)\frac{\partial G(P,Q)}{\partial n_Q} \right) dS(Q), \tag{11}$$

which is a general formulation that is able to model both a pressure jump and a surface velocity jump. The jump formulation Eq. (11) is described in the literature as an alternative to formulations based on the Helmholtz integral equation[13,14], and it is applicable to thin structures frequently appearing in studies of real structures. We can consider Eq. (11) as a formulation based on vibrating thin shells with general impedance boundary conditions on both sides of the shells[15]. The versatility of the general jump formulation Eq. (11), with the ability to handle complex structures, has lead to implementation in many commercial BEM codes, and it is used to study real industrial applications. However, the implementation is not as straightforward as one based on the Helmholtz integral equation.

In the present work we have chosen to work with a hard thin-shell formulation[10] where the quantity $\sigma(Q)$ in Eq. (11) is not necessary, and we thus end up with the double-layer formulation in Eq. (8).

C. Variational solution scheme

In order to establish the forward modelling problem we must derive a complete procedure for computing the field pressure in the exterior region, given the normal surface velocities everywhere on the surface. This is done in two stages. First, the necessary "intermediate" surface quantities must be determined, and then the acoustic field exterior to the source surface is determined from straightforward integration, using one of the above formulations and the appropriate surface quantities. In the direct formulation the pressure on the surface must be determined, and in the indirect formulation the source density (consisting of monopoles and/or

dipoles) must be determined from the known normal surface velocity. In both cases the link between the surface parameters is established from a solution procedure, such as a collocation method or a variational approach.

In this work we have chosen a variational approach to provide the link between the surface parameters. A physical solution at system equilibrium can often be written as the solution that minimizes a certain functional. In relation to finite element analysis, this approach has been applied for decades as the standard method for deriving an associated variational form based on the total potential energy. Minimization of this quantity will determine the solution to the problem. Note that symmetric forms are normally associated with variational principles. Hence, making a functional stationary solves the problem.

We now describe the solution scheme using a variational formulation for the indirect double-layer formulation that we have chosen to work with. The link between normal surface velocities and jump pressures is provided by considering the normal derivative of p_f in Eqs. (8) on the surface. This derivative, in turn, is equal to $-j\omega\rho\,\bar{v}_n(P)$, and we obtain:

$$-j\omega\rho\,\bar{v}_n(P) = \int_S \mu(Q)\frac{\partial^2 G(P,Q)}{\partial n_P \partial n_Q}\,dS(Q)\,, \tag{12}$$

where the surface velocity $\bar{v}_n$ is known.

A functional Π based on energy concepts can be written[10,16] as

$$\Pi = \frac{1}{2}\frac{1}{\rho\omega^2}\int_S\int_S \mu(P)\mu(Q)\frac{\partial^2 G(P,Q)}{\partial n_P \partial n_Q}\,dS(P)\,dS(Q) - \frac{1}{j\omega}\int_S \mu(P)\bar{v}_n(P)\,dS(P)\,. \tag{13}$$

In Gardner et al.[16], Eq. (13) is viewed as the difference between two different representations of the total power. The first term in Π represents the power computed from the pressure jumps, while the second term represents the same power calculated from the boundary condition $\bar{v}_n$. The functional Π to be minimised expresses the difference between these two terms. Making this functional stationary, i.e., $\delta\Pi = 0$, yields

$$-j\omega\rho\int_S \delta\mu(P)\bar{v}_n(P)\,dS(P) = \int_S\int_S \delta\mu(P)\mu(Q)\frac{\partial^2 G(P,Q)}{\partial n_P \partial n_Q}\,dS(P)\,dS(Q)\,. \tag{14}$$

for all $\delta\mu(P)$, where δ denotes 'variation in'.

D. Singularities and irregular frequencies

Singularities appear in every boundary element formulation when the BEM matrices are calculated. This is because the terms associated with Green's function become singular when the observation point P approaches the integration point Q. The best way to deal with this difficulty is to remove the singularities by taking the order of the singularity into account, such that conventional Gauss quadrature can subsequently be used for the numerical integration. For the variational approach a higher order singularity (a so-called hypersingularity) occurs which is reduced to a weak singularity by means of Stoke's theorem[18].

When using BEM techniques in practice, problems may occur due to the mathematical breakdown of the direct or indirect formulation at specific so-called critical or irregular frequencies. These special frequencies are related to eigenfrequencies of the interior region, and will clearly be present if an interior BEM problem is analysed, but they will also affect the results of an exterior BEM analysis if no effort is made to remove their influence. Since meaningless results can occur at the interior eigenfrequencies, we assume throughout this work that such frequencies are avoided. A modified formulation[10] based on Eq. (11), which incorporates absorbing material on the inner surface, can be used to avoid the problems with irregular frequencies; this feature is not included in the present work.

II. THE INVERSE PROBLEM

Whenever a sound source reconstruction problem is discretized – by means of BEM or other discretization methods – a so-called discrete ill-posed problem arises. In this section we describe how to deal with such problems.

The discretized problem can be written in general matrix-vector form as

$$\mathbf{A}\,\mathbf{x} = \mathbf{b}\,, \tag{15}$$

where **A** is a complex transfer matrix of dimension $m \times n$, i.e. m rows and n columns. Hence, the complex vectors **x** and **b** are of dimension n and m, respectively. In the following we assume that the system is either square or over-determined, i.e., $m \geq n$.

In Eq. (15), the matrix **A** represents a model of the system under investigation while **b** is a data vector of known measured values. In our work the system under study is the radiation process from a source to a number of receivers, **b** represents the response at the position of the receivers, and the model represented by **A** should be "inverted" in order to deduce the source descriptors in **x**. We assume that **A** represents an approximation to the actual process, and that the data vector of observed responses is only known with a certain degree of accuracy. We will only consider errors **e** in the right-hand side, while errors in **A** are neglected.

The discrete inverse problem then consists of determining the unknown vector **x** that produces the measured **b**. In principle this could be accomplished by factorisation of **A** followed by the use of a solution approach. Unfortunately, when Eq. (15) arises from discretisation of an inverse problem, **A** will be very ill conditioned. Consequently, a straightforward solution of the discrete inverse problem is not satisfactory. Instead, special techniques should be employed in order to solve Eq. (15) in a near-by sense.

A. Singular value decomposition

Solving discrete ill-posed problems via a direct solution approach should preferably be combined with tools that provide some kind of analysis of the specific problem at hand. Such tools do not solve the problem itself, but will often provide the necessary information before any next step towards a useful solution of the problem is taken. When it comes to ill-conditioned matrices, the ultimate analysis tool seems to be the singular value decomposition (SVD). Given the transfer matrix **A**, we can write the SVD of this matrix[19] as

$$\mathbf{A} = \mathbf{U}\boldsymbol{\Sigma}\mathbf{V}^H, \tag{16}$$

where **U** is a matrix of dimension $m \times n$, **V** is $n \times n$ and $\boldsymbol{\Sigma}$ is a diagonal matrix containing n non-negative values in non-increasing order,

$$\sigma_1 \geq \sigma_2 \geq \cdots \geq \sigma_n \geq 0. \tag{17}$$

These values are called the singular values of **A**. Superscript *H* in Eq. (16) denotes the complex conjugate transposed. This version of the SVD is called the "thin SVD" because the last *m*-*n* columns of **U** are omitted when $m > n$. These columns represent the component of **b** that cannot be reached by any **x** through **A**. The case $m < n$ can be handled by considering the transposed transfer matrix $\mathbf{A}^T$.

The two matrices **U** and **V** are written in the form:

$$\mathbf{U} = \begin{pmatrix} \mathbf{u}_1 & \cdots & \mathbf{u}_n \end{pmatrix} \quad , \quad \mathbf{V} = \begin{pmatrix} \mathbf{v}_1 & \cdots & \mathbf{v}_n \end{pmatrix}, \tag{18}$$

where $\mathbf{u}_i$ (dimension *m*) and $\mathbf{v}_i$ (dimension *n*) are called the left and right singular vectors. An important property of these vectors is their orthonormality, i.e. $\mathbf{U}^H \mathbf{U} = \mathbf{V}^H \mathbf{V} = \mathbf{I}_n$, with $\mathbf{I}_n$ the identity matrix of order *n*.

The condition number (based on the 2-norm) of **A** can be expressed as the ratio of the largest and the smallest singular value[20]

$$\mathrm{cond}\,(\mathbf{A}) = \frac{\sigma_1}{\sigma_n}. \tag{19}$$

This quantity measures a solution's sensitivity to perturbations in the matrix itself as well as in the right-hand side. When we are dealing with ill-conditioned matrices, the range of singular values span many orders of magnitude and **A** is very ill conditioned.

We can write the SVD of **A** in another form:

$$\mathbf{A} = \sum_{i=1}^{n} \mathbf{u}_i \, \sigma_i \, \mathbf{v}_i^H \, . \tag{20}$$

From this expression we see that the transfer matrix **A** is a sum of outer products composed by left singular vectors and their corresponding right singular vector weighted by the singular values. Hence, components corresponding to very small singular values, compared to σ_1, will hardly contribute to the transfer matrix. As a consequence, a badly conditioned matrix **A** may be replaced by a more well-conditioned matrix close to **A** of rank *k*:

$$\mathbf{A}_k = \sum_{i=1}^{k} \mathbf{u}_i \, \sigma_i \, \mathbf{v}_i^H \, . \tag{21}$$

The condition number of this matrix approximation is $\mathrm{cond}(\mathbf{A}_k) = \sigma_1 / \sigma_k$, which can be considerably smaller than the condition number of **A**. The rank *k* may be defined with respect to a

certain threshold, meaning that only singular values strictly larger then the threshold are taken into account. However, if the behaviour of the singular values show no significant gap between large and small values, it is difficult to determine k via a threshold. On the other hand, some kind of filtering of the singular values must be added to the original problem before any solution step makes sense.

The behaviour of the left and right singular vectors deserves special attention, because any filtering relies on this behaviour. Hansen[20] has demonstrated that the left and right singular vectors tend to have more oscillations as the index i increases when the transfer matrix arises from discretisation of an inverse problem. Thus we will assume that high-frequency information is linked to left- and right singular vectors having high index i. Likewise, the vectors with small index represent slowly varying functions having few sign-changes. These considerations have not been proven, but for practical problems derived from integral equations they appear to be valid.

B. Tikhonov regularisation

If all SVD-components are taken into account, a very oscillating solution with a huge norm is obtained whenever the error component **e** of the right-hand side **b** is dominant for high indices – and this is almost always the case. One way of suppressing the disastrous influence of these errors is to solve the initial ill-conditioned problem in a near-by sense with a side constraint on the size of the sought solution. The solution size is linked to the solution smoothness, because ignoring components with high index will lead to a smooth solution with reasonable size as measured by an appropriate norm.

In mathematical form, we can write this as a minimisation problem where the functional to be minimised involves a residual norm and a smoothing norm $\Omega(\cdot)$ acting on the solution vector:

$$\min_{\mathbf{x}} \left\{ \left\| \mathbf{A}\,\mathbf{x} - \mathbf{b} \right\|_2^2 + \lambda^2 \Omega(\mathbf{x})^2 \right\}. \tag{22}$$

Here, the regularisation parameter λ is the only input when a suitable smoothing norm has been defined. If $\lambda = 0$ we obtain the least-squares problem and the unregularised solution is computed. A large λ favours a small solution size at the cost of a large residual norm. Hence, λ controls the degree to which the sought regularised solution should fit to the measured data in **b** or have small solution size. Clearly, solving Eq. (22) involves a trade-off between the residual norm and the

solution size, and this is determined by the single parameter λ. This form of regularisation is known as Tikhonov regularisation, which is discussed at length, e.g., in Hansen[20]. In order to solve Eq. (22), we use a discrete smoothing norm of the form $\Omega(\mathbf{x}) = \|\mathbf{L}\,\mathbf{x}\|_2$ where $\mathbf{L}$ is a $p \times n$ real regularisation matrix with $p \le n$. This leads to the problem

$$\min_{\mathbf{x}} \left\{ \|\mathbf{A}\,\mathbf{x} - \mathbf{b}\|_2^2 + \lambda^2 \|\mathbf{L}\,\mathbf{x}\|_2^2 \right\}, \tag{23}$$

We note that while the residual usually is measured by the 2-norm, it is often advantageous to use other norms to measure the size of the solution; for example, the 1-norm may be a good choice for producing a discontinuous solution[20]. We return to our choice of $\mathbf{L}$ later.

In order to find the minimum of Eq. (23) we can formulate the Tikhonov problem as[20]

$$\left(\mathbf{A}^H \mathbf{A} + \lambda^2 \mathbf{L}^T \mathbf{L}\right)\mathbf{x}_\lambda = \mathbf{A}^H \mathbf{b}\,, \tag{24}$$

whose solution is given by

$$\mathbf{x}_\lambda = \left(\mathbf{A}^H \mathbf{A} + \lambda^2 \mathbf{L}^T \mathbf{L}\right)^{-1} \mathbf{A}^H \mathbf{b}\,, \tag{25}$$

where the subscript λ is used to emphasise the dependence of the solution on the regularisation parameter. We see that the inverse of the ill-conditioned transfer matrix is replaced by the Tikhonov regularised inverse of the transfer matrix, $\left(\mathbf{A}^H \mathbf{A} + \lambda^2 \mathbf{L}^T \mathbf{L}\right)^{-1} \mathbf{A}^H$.

When $\mathbf{L} = \mathbf{I}_n$, the Tikhonov regularised solution can be written conveniently in terms of the SVD of $\mathbf{A}$ as

$$\mathbf{x}_\lambda = \sum_{i=1}^{n} \frac{\sigma_i^2}{\sigma_i^2 + \lambda^2} \frac{\mathbf{u}_i^H \mathbf{b}}{\sigma_i} \mathbf{v}_i\,. \tag{26}$$

The filtering is described by the filter factors $f_i = \sigma_i^2 / (\sigma_i^2 + \lambda^2)$. In practice, the regularisation parameter is chosen to lie between the highest and smallest singular value. Hence,

$$f_i(\lambda) \approx \begin{cases} 1 & \lambda \ll \sigma_i \\ \frac{1}{2} & \lambda = \sigma_i \\ (\sigma_i / \lambda)^2 & \lambda \gg \sigma_i \end{cases}. \tag{27}$$

Clearly, the filter gradually removes the singular values smaller than λ.

C. Parameter-choice methods

The main difficulty with regularisation methods is that a proper choice of the amount of regularisation is not easily found. Choosing the continuous parameter λ in Tikhonov regularisation is not straightforward. Ideally, we would like to determine the regularisation parameter such that the computed regularised solution provides the best possible estimate of the exact solution $\mathbf{x}^{exact}$. Closeness can here be measured by a vector-norm, e.g., a 2-norm. This leads to the following minimisation problem:

$$\min_{\lambda} \left\{ \left\| \mathbf{x}^{exact} - \mathbf{x}_{\lambda} \right\|_2 \right\}. \tag{28}$$

From Eq. (28), we obtain the optimal regularisation parameter according to the defined measure of closeness. The only problem is that the exact solution is not available. However, parameter-choice methods should be able to compute regularisation parameters that are good approximations to the optimal ones.

Parameter choice methods, which do not require information about the error-norm $\|\mathbf{e}\|_2$ are preferred whenever reliable information about $\|\mathbf{e}\|_2$ is not available. Here we consider two error-free methods for extracting an optimal regularisation parameter. The first method, which is very popular, is called generalised cross-validation (GCV). It is based on the philosophy that an arbitrary element b_i of the right-hand side should be predicted well by the regularised solution, when this element is left out of the inverse problem. This method works well if the noise is spatially white, i.e., if the elements of the noise vector are unbiased and have the same variance.

Another $\|\mathbf{e}\|_2$-free approach to estimating the regularisation parameter in Tikhonov regularisation is the so-called L-curve criterion. The idea behind the L-curve is to plot the discrete smoothing norm of the regularised solution versus the residual norm in a log-log scale, for all valid regularisation parameters. In Fig. 2, the generic form of the L-curve is plotted. The smoothing norm is here $\|\mathbf{L}\,\mathbf{x}_{\lambda}\|_2$ and the residual norm is $\|\mathbf{A}\,\mathbf{x}_{\lambda} - \mathbf{b}\|_2$, i.e., the two terms occurring in the functional to be minimised in Tikhonov regularisation. The shape of the L-curve can be explained by considering its different sections. The horizontal part of the curve is characterised by solutions that have been smoothed too much (over-regularised), whereas the vertical part is characterised by solutions dominated by the effects of errors (under-regularised). In between these parts, we find solutions representing a balance between fitting the solution to data and keeping the

solution's smoothing norm small. The optimum value of the regularisation parameter defined by the L-curve criterion is at the corner of the curve, where we find a solution that has a reasonably small residual as well as a reasonably limited smoothing norm. We note that this is only possible in a plot in log-log scale[21].

III. IMPLEMENTATION OF THE INVERSE SOURCE PROBLEM

The inverse of the radiation process is the starting point when formulating the inverse problem of reconstructing the surface velocity distribution from the measured field pressures. Instead of referring to an inverse radiation process, we will specifically characterise it as an inverse source problem, to emphasise that the goal is not only to invert the radiation process, but also to reconstruct the source by means of a boundary element model. The procedure for extracting the source data from the field data is described below.

Integral formulations are usually implemented numerically by a boundary element method (BEM) where the surface of the boundary is replaced by a multitude of elementary segments. These surface elements can be either triangles or squares, and the associated interpolation functions for the source values are typically linear or quadratic. In the present study triangular linear elements are used for describing the geometry as well as the acoustic variables on the surface. Hence, linear interpolation is used throughout for the geometry as well as the acoustic parameters, and the elements are therefore isoparametric, i.e., the same order of shape function is used in both cases. We note the general rule of thumb that the element size should not exceed one fourth of the shortest wavelength for the linear elements.

First we derive the set of matrix equations needed to formulate the inverse problem, and we define the transfer matrix associated with the problem. The matrices are easily computed by means of the developed indirect BEM implementation. Subsequently, we will establish a functional amenable to Tikhonov regularisation which will be the type of regularisation imposed on the problem. While the set-up of the discrete inverse problem is rather simple, solving it requires special attention owing to the ill-posed nature of the underlying problem. Since the modeling of the inverse problem is linked to the BEM in acoustics, we will use the term Inverse Boundary Element Method (IBEM) or inverse BEM, to emphasize the difficult nature of the inverse problem associated with this method.

A. Formation of the inverse BEM transfer matrix

Since we use an indirect BEM formulation, we can sketch the fundamental set-up for the IBEM reconstruction as illustrated in Fig. 3. In this figure, a closed structure is shown, but we emphasize that the formulation will work for an open structure as well. Since the implemented BEM formulation is also known as a thin-shell formulation, the structure is depicted with a surface pressure-jump. The normal vector on the surface S points into the exterior. We will assume that N_m microphones are situated in the exterior region of the source. Basically these microphones can be located anywhere in this region, but some locations may be preferred over others. For every microphone position we will then measure an acoustic pressure.

We now turn to the discretization of Eqs. (8) and (14) by means of BEM. The goal is to link the N_m measured field pressures to an acoustic quantity on the source surface. From the indirect formulation we first establish the relation between the field pressures p_f and the pressure-jump μ on the source surface by discretisation of the integral representation Eq. (11). For each boundary element we introduce the vectors $\mathbf{N}_i$ and $\boldsymbol{\mu}_i$ which represent the surface geometry and the nodal values of the pressure-jump distribution, respectively. This leads to the discretized problem

$$p_f(P) = \sum_{i=1}^{N_e} \int_{S_i} \mathbf{N}_i^T \boldsymbol{\mu}_i \frac{\partial G(P,Q)}{\partial n_Q} dS_i(Q), \tag{29}$$

where N_e is the number of boundary elements.

For each measurement point we now use Eq. (29) to express the measured field p_f in terms of the nodal values of the pressure jumps. The integrals in Eq. (29) can be evaluated using standard Gauss quadrature, as long as the point P is not too close to the source surface. The minimum distance between field points and source surface for BEM calculations is normally set to an element length[22]. Expressed in matrix-vector form the discretized problem becomes

$$\mathbf{p}_f = \mathbf{G}\,\boldsymbol{\mu}, \tag{30}$$

where $\mathbf{p}_f$ is a complex vector containing the N_m field pressure values at a specific frequency, and $\boldsymbol{\mu}$ is a vector with the pressure-jump values on the discretised surface containing N_n nodes. The

$N_m \times N_n$ transfer matrix **G** is notoriously ill conditioned.

Rather than solving Eq. (30) for $\boldsymbol{\mu}$ given a known vector $\mathbf{p}_f$, we will relate the field pressure vector to the normal surface velocity vector $\mathbf{v}_n$. This is done by means of the relation between pressure-jump and normal surface velocity from the indirect boundary element formulation Eq. (14). which, when discretized, takes the form

$$-j\omega\rho\,\boldsymbol{\delta\mu}^T\left(\int_S \mathbf{N}\cdot\mathbf{N}^T\,dS(P)\right)\mathbf{v}_{\mathrm{n}} = \boldsymbol{\delta\mu}^T\left(\int_S\int_S \mathbf{N}\frac{\partial^2 G(P,Q)}{\partial n_P \partial n_Q}\mathbf{N}^T\,dS(P)dS(Q)\right)\boldsymbol{\mu}, \qquad (31)$$

or in matrix-vector form,

$$-j\omega\rho\,\mathbf{B}\,\mathbf{v}_{\mathrm{n}} = \mathbf{Q}\,\boldsymbol{\mu}. \qquad (32)$$

The two matrices **B** and **Q** are symmetric, i.e., $\mathbf{B}=\mathbf{B}^T$ and $\mathbf{Q}=\mathbf{Q}^T$. Moreover **B** is real-valued and sparse, while **Q** is complex and full. Note that the evaluation of the coefficients in the **Q**-matrix is not trivial due to the hyper-singular kernel that must be treated specially[10].

We note that the BEM matrices are always full. This is a result of the method itself being non-local and thus coupling every unknown with all the other unknowns throughout the boundary. Domain decomposition methods based on infinite elements result in localised symmetric systems with a sparse matrix. However, despite the attractive properties of such infinite boundary element integral equations, these methods are not widely used yet.

Combining Eqs. (30) and (32) we then obtain

$$\mathbf{p}_f = -j\omega\rho\,\mathbf{G}\,\mathbf{Q}^{-1}\,\mathbf{B}\,\mathbf{v}_n = \mathbf{H}\,\mathbf{v}_n. \qquad (33)$$

Here, we have introduced the $N_m \times N_n$ rectangular transfer matrix, $\mathbf{H} = -j\omega\rho\,\mathbf{G}\,\mathbf{Q}^{-1}\,\mathbf{B}$, which is further analysed in our IBEM problems.

Since **G** is ill-conditioned for measurement points lying strictly in the exterior, this property is carried over to the transfer matrix **H**, relating normal surface velocity at nodes to acoustic pressure at measurement points. Moreover, there is a unique relationship between pressure-jumps $\boldsymbol{\mu}$ and normal surface velocity $\mathbf{v}_n$ as long as the frequency is not irregular for the problem. Consequently, Eq. (33) represents a discrete ill-posed problem of the form studied in section II. Note that the assembly of **H** necessitates the inverse of **Q**, which will not cause trouble as long we

avoid irregular frequency (interior Neumann eigenfrequencies) for a closed structure. How to solve Eq. (33) in the near-by sense by formulating a Tikhonov problem is discussed next.

B. Tikhonov problem

The regularisation imposed in this investigation is based on Tikhonov's method with a parameter-choice method to estimate the optimal regularisation parameter. In general form, the minimisation problem for Tikhonov regularisation is written as

$$\min_{\mathbf{v}_n} \left\{ \left\| \mathbf{H}\,\mathbf{v}_n - \mathbf{p}_f \right\|_2^2 + \lambda^2 \left\| \mathbf{L}\,\mathbf{v}_n \right\|_2^2 \right\}. \tag{34}$$

The discrete smoothing norm $\Omega(\mathbf{v}_n) = \left\| \mathbf{L}\,\mathbf{v}_n \right\|_2$ must be chosen to preferably reflect some physical quantity to be penalised, that is, to have limited size. One such quantity could be some type of energy associated with a vibrating thin shell since the model is based upon shells. The equivalent kinetic energy of the entire shell structure makes sense, since the size of this quantity will increase dramatically if the non-radiating components have too large influence on the regularised solution.

The "kinetic energy smoothing norm" is derived by considering the squared surface velocity over the shell surface. Since we only have access to the normal component of surface velocity, the equivalent total kinetic shell energy is written as

$$\int_S \left| v_n \right|^2 dS = \int_S v_n\, v_n^* \, dS\,, \tag{35}$$

where the asterisk denotes 'complex conjugate'. We can discretise this quantity using standard Gaussian quadrature and the discretisation of Eq. (35) may be written

$$\int_S \mathbf{v}_{n,i}^H \mathbf{N}_i \mathbf{N}_i^T \mathbf{v}_{n,i}\, dS = \mathbf{v}_n^H\, \mathbf{B}\, \mathbf{v}_n\,, \tag{36}$$

with the shape function vector $\mathbf{N}_i$ for each element and $\mathbf{B}$ is similar to the one defined via Eq. (31).

To simplify the calculations in the Tikhonov regularisation, we may approximate the total surface function $v_n\, v_n^*$ as a linear function. Consequently, we end up with a diagonal matrix $\mathbf{D}$ that can be considered as an approximation to $\mathbf{B}$. Using this approach the surface integral is written

$$\mathbf{v}_n^H \left(\int_S \mathrm{diag}(\mathbf{N}_i)\, dS \right) \mathbf{v}_n = \mathbf{v}_n^H\, \mathbf{D}\, \mathbf{v}_n\,. \tag{37}$$

Here the integrand is a sum of element areas weighted by the shape functions. Hence, only one Gauss point for each element integration is required. For each element integration over S_i, the value $\frac{1}{3} S_i$ is added on the diagonal of the area matrix for each node participating in element i. As a result, the diagonal element of $\mathbf{D}$ corresponding to a node in the BEM model will contain one third of the total element areas for which this node is part of. Thus, the kinetic energy smoothing norm simply introduces an area weighting of the nodal values. The discrete smoothing norm is now written as

$$\mathbf{v}_n^H \, \mathbf{D} \, \mathbf{v}_n = \left\| \mathbf{D}^{\frac{1}{2}} \, \mathbf{v}_n \right\|_2^2, \tag{38}$$

where the regularisation matrix $\mathbf{D}^{\frac{1}{2}}$ is found by taking the square root of all the diagonal entries. In general, though, if our matrix were not diagonal, e.g. like $\mathbf{B}$, we would have to factorise using Cholesky factorisation to obtain $\mathbf{L}$. Notice that if the element size is almost constant over the entire mesh surface, $\mathbf{D}$ will be close to the identity matrix except for a multiplication constant. In that case, the standard form ($\mathbf{L} = \mathbf{I}_n$) of Eq. (34) could equally be used. However, for a general mesh, which could be finer for some surface regions $\mathbf{D}^{\frac{1}{2}}$ from Eq. (38) should be used instead of the identity matrix. For that reason, the general form Tikhonov regularisation is rewritten in standard form and solved.

IV. CASE STUDIES

In order to demonstrate the capabilities of inverse BEM, some real-life applications have been studied[10]. The sound sources considered and modelled are based on a real tyre on a drum. The tyre is a standard tyre for passenger cars and its characteristics as a source were studied as a standing tyre excited by a shaker as well as a rolling tyre at 80 km/h. Both cases are illustrated in Fig. 4.

A. Tyre measurements

The measurements were recorded using a planar microphone array for the side measurements, and a curved array for close measurements at the front and the rear of the tyre. Moreover, four reference microphones were distributed around the tyre in order to derive a principal component description of the sound field. Two of these four reference microphones were placed on the ground in front of and behind the tyre, while the other two microphones were located in the air above the tyre. When dealing with Cross Spectral holography techniques and sound radiation from tyres, four reference microphones seem to be sufficient[23]. Measurements were made in 821 positions for the shaked tyre and 977 for the rolling tyre. In addition to the IBEM reconstructions, we processed the data recorded at the tyre side using Near-field Acoustic Holography as implemented in the Brüel & Kjær STSF[24,25] system. This allows for a comparison of the transformed sound fields obtained using IBEM and STSF. For example we can compare the source reconstruction on the tyre side-wall performed by the two methods[26,27].

In order to model the acoustic environment, a combined model with the tyre attached to the drum was made. Since the hard ground is modelled by introducing an infinite plane, we only need to model and mesh the surface of the drum and the part of the tyre that is not in contact with the ground. The meshed model is shown in Fig. 5; notice that 105 of the total 371 nodes belong to the drum.

B. Standing tyre excited by a shaker

First, we use the BEM model to study the inverse BEM problem for the shaked tyre at a low frequency, 100 Hz. Since the boundary element nodes associated with the drum are non-vibrating, we impose a zero surface velocity boundary condition on these 'rigid' nodes. This can be done by setting up the transfer matrix relating all measurement positions to all nodes, and then discard the columns of the transfer matrix corresponding to 'rigid' nodes. The transfer matrix is then of size 821×266 for the shaked tyre.

For the tyre side, a 6 x 6 array was scanned across a plane area with dimensions 1.7 m x 0.9 m. The microphone spacing in the horizontal and vertical direction was 0.05 m giving a total of

665 measurement points in the plane, which was located 0.07 m from the side wall of the tyre. In addition, a curved array of 12 microphones scanned the rear of the tyre, the shaker excitation being on the front. The curved array was scanned across the curved surface in 13 steps with a step size of 0.05 m, thus giving 156 measurement points. The distance between the curved array and the curved part of the tyre was about 0.07 m. The front of the tyre was not measured, as the shaker occupied part of the space there.

Each principal hologram can now be considered as a field pressure distribution and we can process the holograms individually, since they are mutually independent (incoherent). That is, for each principal hologram we determine a regularised surface velocity distribution by means of the L-curve criterion. The L-curve for the principal hologram corresponding to the largest principal auto-power at 100 Hz is shown in Fig. 6. This L-curve exhibits the generic shape of Fig. 2 with a well-defined corner.

The computed regularised surface velocity solution for each principal component represents a principal source related to the vibrating tyre structure. The total surface velocity level is obtained by summing the principal component contributions on a power basis, subject to a Wiener type of filter controlled by the principal auto-powers. This total surface velocity distribution is shown on the tyre model in Fig. 7. Note that only the highest 20dB of the available data are plotted. Since we can observe the tyre from any position, we can look at the spot where the shaker excites the tyre. This reveals a significant hot spot associated with maximum vibration level.

In order to compare the sound field reconstructions obtained by IBEM and STSF, the sound pressure and the particle velocity was computed on a plane close to the tyre side-wall. Using STSF, this was done by processing the measurement data from the plane array measurement at the tyre side, and then backward propagating the acoustic field 0.05 m onto a plane close to the tyre side. When using IBEM with the L-curve criterion, the principal holograms were processed independently in order to obtain a set of principal sources. These sources were then processed as part of a forward BEM problem for computing the normal component of the particle velocity and the acoustic pressure over the same plane as in the STSF computation. Furthermore, in order to assess the L-curve criterion, a similar calculation was made using the GCV criterion for each principal component. The particle velocity and pressure distributions obtained by these two different IBEM calculations are shown in Fig. 8 together with the result of the STSF calculation. Both the sound pressure level distributions and the particle velocity distributions obtained by STSF

and by IBEM (L-curve), see Fig. 8, agree very well. The levels are almost identical. The GCV results, on the other hand, are completely off with a level about 40 dB too high. Clearly, the L-curve criterion applied to each principal component leads to a useful reconstructed particle velocity distribution while the GCV criterion computes too small regularisation parameters resulting in under-smoothed solutions completely dominated by measurement errors. In other words, the GCV criterion applied to our case fails to provide a useful reconstruction.

It is likely that the GCV-based regularisation fails because the measurement errors are rather far from being spatially white. We mention two types of such errors:

1. Transducer mismatch. These errors "follow" the array transducers during the scanning, and the resulting errors in the measured sound pressure will therefore be correlated with the true sound pressure.
2. Transducer position errors. The measurement positions are never exactly known in the coordinate system of the BEM model. The resulting errors in the measured pressure will also tend to be correlated with the true pressure.

The L-curve criterion does not rely in the same way on the noise being spatially white as GCV does. Practical IBEM problems in acoustics will not typically suffer from only spatially white noise, so the L-curve approach seems better suited to solve such problems.

In the present case of the shaked tyre, the sound field should be perfectly coherent, apart from background noise and effects of non-linearities. So it would have been sufficient to use only a single reference signal. Use of four reference signals leads to a set of principal components with one dominating component and three low-level components dominated by noise. The three components dominated by noise represent a challenge to the applied regularisation schemes. The solutions of Figs. 7 and 8 obtained by STSF and by IBEM (L-curve) are dominated by the first principal component with the highest principal auto-power.

C. Rolling tyre

The same analysis is carried out for the rolling tyre case. One major difference between the two measurement cases is that the rolling tyre measurement includes a curved array scanning of the tyre front, thus providing more information about the total sound field around the rolling tyre. Again, this curved array was located 0.07 m from the tyre and scanned with a step-size of 0.05 m.

By adding these front measurement positions to the plane and curved array measurement positions from the shaked tyre set-up, we end up with a total of 977 measurement points.

Using the same set of four reference microphones, a principal component description of the sound field was derived. Again, we use a very low frequency, this time corresponding to a band of width 20 Hz centered at 60 Hz, and we impose the zero surface velocity boundary condition on the 'rigid' nodes belonging to the drum. This gives us a 977×266 transfer matrix for the rolling tyre.

Each of the four principal holograms at 60 Hz is again associated with an inverse problem. Compared to the shaked tyre measurement, we will now for the rolling tyre expect some additional errors arising from the rotating drum producing background noise, as well as wind noise induced in the microphones due to wind from the fast rotating tyre. However, these additional error components will be rather uncorrelated with the noise radiated from the tyre, so provided they are not too large they are not expected to cause major additional problems. A major difference from the case of the shaked tyre measurement is that now we will have four significant principal components – all four containing information about the noise due to tyre vibration.

The reconstructed surface velocity level distribution is shown in 3D in Fig. 9. Figure 10 shows the pressure and the particle velocity level distributions on a plane surface close to the tyre side-wall, calculated with the aid of STSF, IBEM (L-curve) and IBEM (GCV). Again, it is found that the L-curve criterion provides reconstructions that are comparable to the STSF calculations - as opposed to the IBEM reconstruction obtained by the GCV method. The pressure levels predicted by STSF and by IBEM (L-curve) are almost identical. But for the particle velocity, IBEM (L-curve) predicts a level at least 10 dB higher than the STSF prediction. This is because IBEM with the L-curve criterion allows a dynamic range in the computed velocity that is approximately 10 dB higher than the dynamic range specified to the STSF program. Recall that the pressure field (over the reconstruction plane) can be formulated as a spatially low-pass filtered version of the particle velocity field. Hence the increased dynamic range in the IBEM reconstruction affects the velocity prediction more than the pressure prediction, because the velocity reconstruction requires more amplification of high spatial frequencies than the pressure reconstruction. These considerations illustrate how useful the automatic ($\|\mathbf{e}\|_2$-free) detection of the applicable dynamic range is. The solutions obtained by the use of GCV are again completely dominated by errors, and the levels are approximately 40 dB too high.

V. CONCLUSIONS

A model of an inverse acoustic source problem was made using the indirect variational BEM formulation described in the first part of the paper. A transfer matrix relating field pressures to surface velocities was formed to take part in a Tikhonov regularisation problem. The crucial part associated with choosing the optimal amount of regularisation was discussed in the context of error-free parameter-choice methods. The optimal amount of regularisation was estimated using the L-curve criterion as well as the popular GCV-method for two different tyre applications. In both cases we compared reconstructed acoustic field quantities on a plane surface close to the tyre side with data from near-field acoustic holography (STSF). In all our experiments, the L-curve criterion provided realistic source reconstructions. The reconstructed source distributions computed by means of GCV were less satisfying as a result of the complicated error distributions contaminating the measured data. While the GCV method is well established for reconstruction in the presence of spatially white noise, the cases investigated in this work demonstrate that the L - curve method may be a better choice for practical measurements, where correlated measurement errors such as transducer phase and position errors are present. As a consequence, the L-curve criterion seems to be more robust than the GCV for estimating the optimal amount of regularisation.

REFERENCES

[1] F. Augusztinovicz and M. Tournour, *Reconstruction of source strength distribution by inversing the boundary element method*, in O. von Estorff (Ed.), Boundary Elements in Acoustics (WIT Press, 2000).

[2] M. R. Bai, "Application of BEM (boundary element method)-based acoustic holography to radiation analysis of sound sources with arbitrarily shaped geometries," *J. Acoust. Soc. Am.*, **92**, 533-549 (1992).

[3] G.-T. Kim & B.-H. Lee, "3-D Sound source reconstruction and field reprediction using the Helmholtz integral equation," *J. Acoust. Soc. Am.*, **136**, 245-261 (1990).

[4] W. A. Veronesi & J. D. Maynard, "Digital holographic reconstruction of sources with arbitrarily shaped surfaces," *J. Acoust. Soc. Am.*, **85**, 588-598 (1989).

[5] R. Martinez, "The Thin-shape Breakdown (TSB) of the Helmholtz Integral Equation," *J. Acoust. Soc. Am.*, **90**, 2728-2738 (1991).

[6] V. Cutanda, P. M. Juhl & F. Jacobsen, "On the modeling of narrow gaps using the standard BEM," *J. Acoust. Soc. Am.*, **109**, 1296-1303 (2001).

[7] P. J. T. Filippi, "Layer Potentials and Acoustic Diffraction," *J. Sound Vib.*, **54**, 473-500 (1977).

[8] L. H. Chen & D. G. Schweikert, "Sound Radiation from an Arbitrary Body," *J. Acoust. Soc. Am.*, **35**, 1626-1632 (1963).

[9] L. G. Copley, "Fundamental Results Concerning Integral Representations in Acoustic Radiation," *J. Acoust. Soc. Am.,* **44**, 28-32 (1968).

[10] A.P. Schuhmacher, "Sound source reconstruction using inverse sound field calculations," Ph.D. thesis, Dept. of Acoustic Technology, Technical University of Denmark, Report 77 (2000).

[11] M. N. Sayhi, Y. Ousset & G. Verchery, "Solution of Radiation Problems by Collocation of Integral Formulations in Terms of Single and Double Layer Potentials," *J. Sound Vib.*, **74**, 187-204 (1981).

[12] X. Zeng, J. Bielak & R. C. MacCamy, "Unified Symmetric Finite Element and Boundary Integral Variational Coupling Methods for Linear Fluid-Structure Interaction," *Num. Meth. Part. Diff. Eq.*, **8**, 451-467 (1992).

[13] O. von Estorff, A. Homm & F. Bartels, "Sound Radiation of a Cantilever Plate – Comparisons of BEM Results with Experimental Data," Betech 91, Southampton, 1991.

[14] O. von Estorff, M. Fischer & W. J. M. Keiper, "Sound Radiation of a Tuning-fork by Boundary Elements," BEM 14, Seville, 1992.

[15] S. T. Raveendra, N. Vlahopoulos & A. Glaves, "An Indirect Boundary Element Formulation for Multi-valued Impedance Simulation in Structural Acoustics," *App. Math. Modelling*, **22**, 379-393 (1998).

[16] B. K. Gardner, J. S. Bolton, S. T. Raveendra & N. Vlahopoulos, "Radiation Efficiency Calculations for Verification of Boundary Element Acoustic Codes," *Noise Control Eng. J.*, **44**, 215-223 (1996).

[17] R. Jeans & I. C. Mathews, "A Comparison of Numerical Collocation and Variational Procedures to the Hypersingular Acoustic Integral Operator," *Comp. Meth. App. Mech. Eng.*, **101**, 5-26 (1992).

[18] M. A. Hamdi, "Une Formulation Variationnelle par Equations Integrales pour la Resolution de l'equation de Helmholtz avec des Conditions aux Limites Mixtes," C. R. Acad. Sc. Paris, Ser. II, **292**, 17-20 (1981).

[19] G. H. Golub and C. F. van Loan, *Matrix Computations* (The John Hopkins University Press, Baltimore, 1996).

[20] P. C. Hansen, *Rank-Deficient and Discrete Ill-Posed Problems* (SIAM, Philadelphia, 1998).

[21] P. C. Hansen & D. P. O'Leary, "The use of the L-curve in the regularisation of discrete ill-posed problems," *SIAM J. Sci. Comput.*, **14**, 1487-1503 (1993).

[22] I-DEAS Vibro-Acoustics™, User's Manual, Version 5.0, 1997.

[23] H.-S. Kwon, J. S. Bolton and D. L. Hallman, "Nearfield Acoustical Holography applied to sound radiation from tires," *Proceedings Noise-Con '98*, Ypsilanti, 1998.

[24] J. Hald, "STSF – a unique technique for scan-based near-field acoustic holography without restrictions on coherence," Brüel & Kjær Technical Review no. 1, 1989.

[25] J. Hald, "STSF – a unique technique for scan-based near-field acoustic holography without restrictions on coherence," Brüel & Kjær Technical Review no. 2, 1989.

[26] A. Schuhmacher, J. Hald and E.-U. Saemann, "A comparison of inverse boundary element method and near-field acoustical holography applied to sound radiation from a tyre," *Proceedings Sixth International Congress on Sound and Vibration*, Copenhagen, 1999.

[27] A. Schuhmacher, "Practical application of inverse boundary element method to sound field studies of tyres," *Proceedings Internoise '99*, Ft. Lauderdale, 1999.

FIGURE CAPTIONS

Figure 1. Definition of geometry in the radiation problem. A 3-D structure with boundary S is immersed in a fluid. The exterior region of the structure is denoted Ω^+ and a vector normal to the surface S pointing into the exterior region is shown as $\mathbf{n}$. Two points in space are defined: P is an observation point in Ω^+ and Q a point on the surface S. The distance between P and Q is denoted R.

Figure 2. The generic L-curve; a plot in log-log scale of discrete smoothing norm vs. the residual norm as a function of regularisation parameter λ.

Figure 3. Sketch of IBEM configuration with sensors (microphones) situated in the exterior of the source surface *S*, which is modelled as a thin shell.

Figure 4. Two different measurement configurations; a) standing tyre excited by a shaker, b) rolling tyre on drum.

Figure 5. Boundary element model of tyre attached to drum (712 triangular elements, 371 nodes).

Figure 6. L-curve corresponding to the principal hologram having the largest principal auto-power for the shaked tyre at 100 Hz.

Figure 7. Reconstructed surface velocity for shaked tyre at 100 Hz computed by IBEM (L-curve criterion). Only the top 20 dB is displayed.

Figure 8. Reconstructed acoustic fields close to the tyre side for the shaked tyre at 100 Hz. The top 20 dB is displayed with a contour interval of 2 dB.

Figure 9. Reconstructed surface velocity for rolling tyre at 60 Hz computed by IBEM (L-curve criterion). Only the top 20 dB is displayed.

Figure 10. Reconstructed acoustic fields close to the tyre side for a rolling tyre at 60 Hz. The top 20 dB is displayed with a contour interval of 2 dB.

FIGURE 1

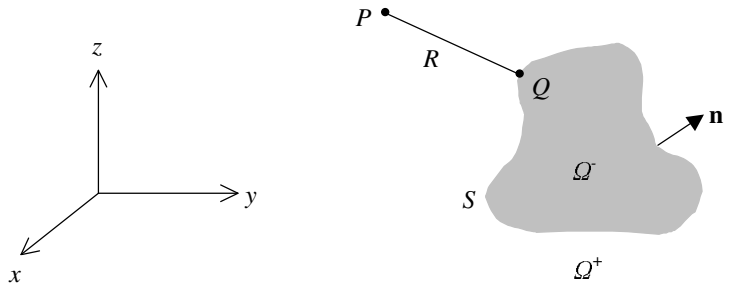

FIGURE 2

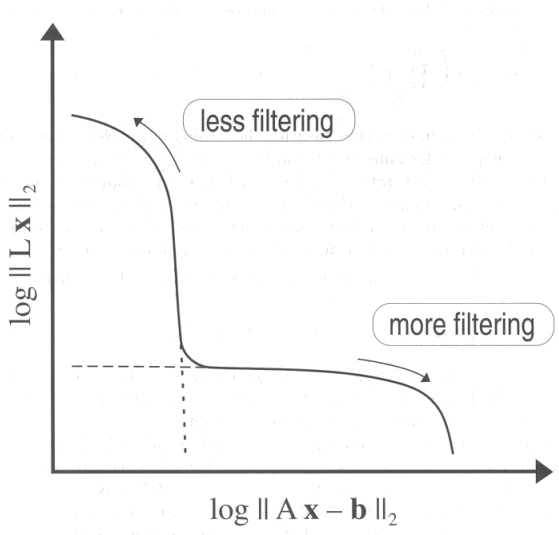

FIGURE 3

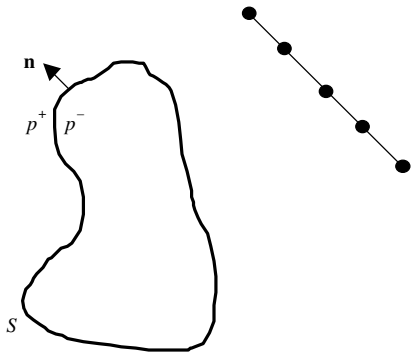

- N_e boundary elements
- N_n boundary nodes
- N_m sensors (microphones)

FIGURE 4

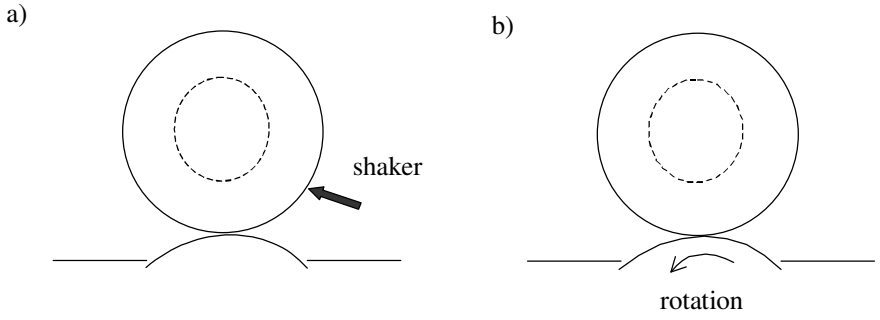

FIGURE 5

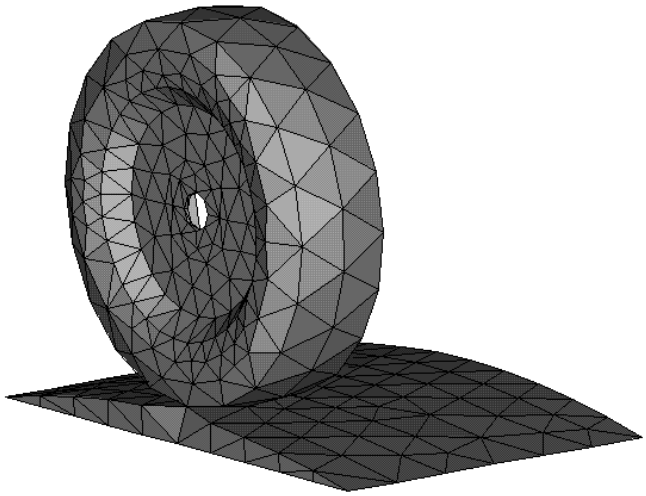

FIGURE 6

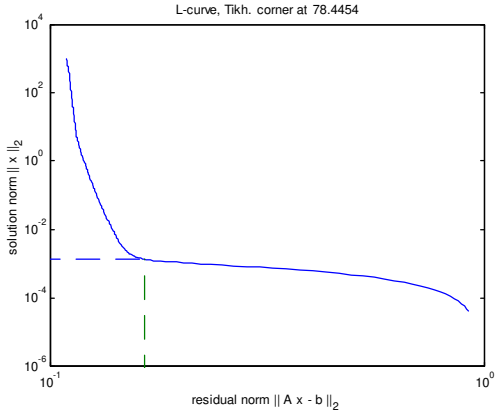

FIGURE 7

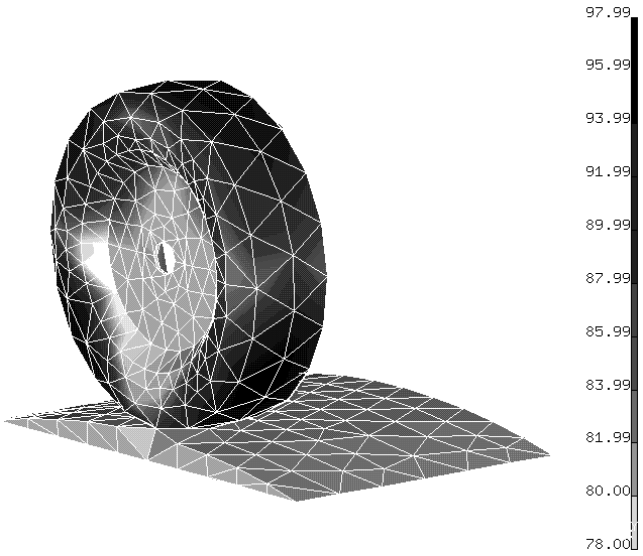

FIGURE 8

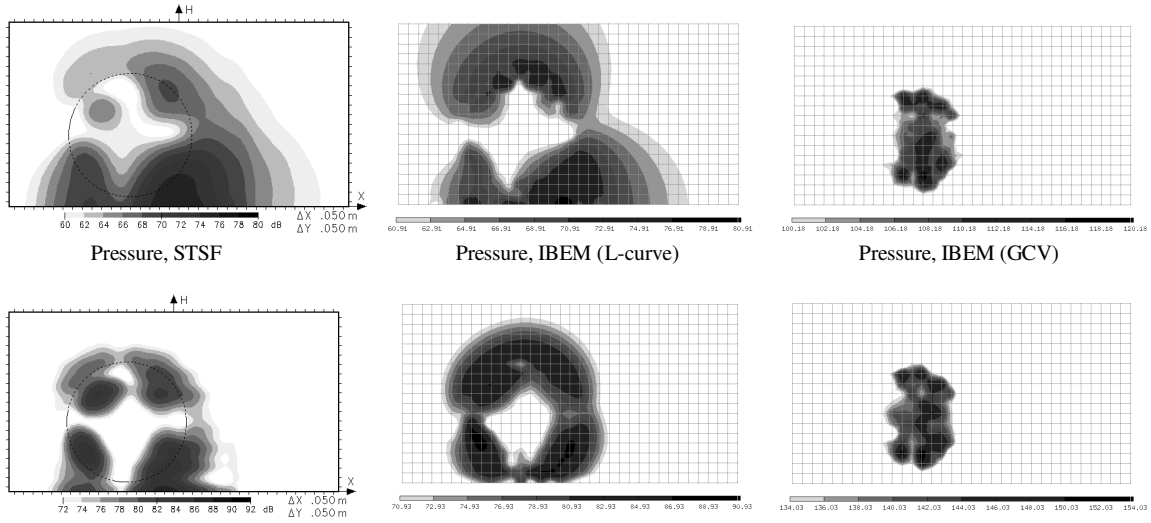

Pressure, STSF | Pressure, IBEM (L-curve) | Pressure, IBEM (GCV)

Particle velocity, STSF | Particle velocity, IBEM (L-curve) | Particle velocity, IBEM (GCV)

FIGURE 9

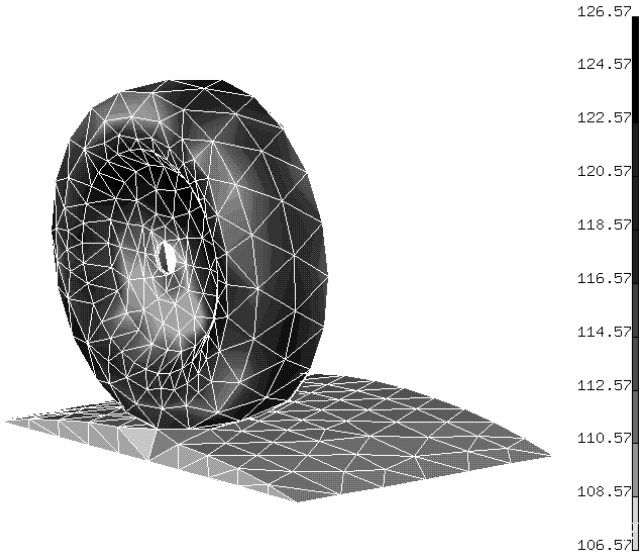

FIGURE 10

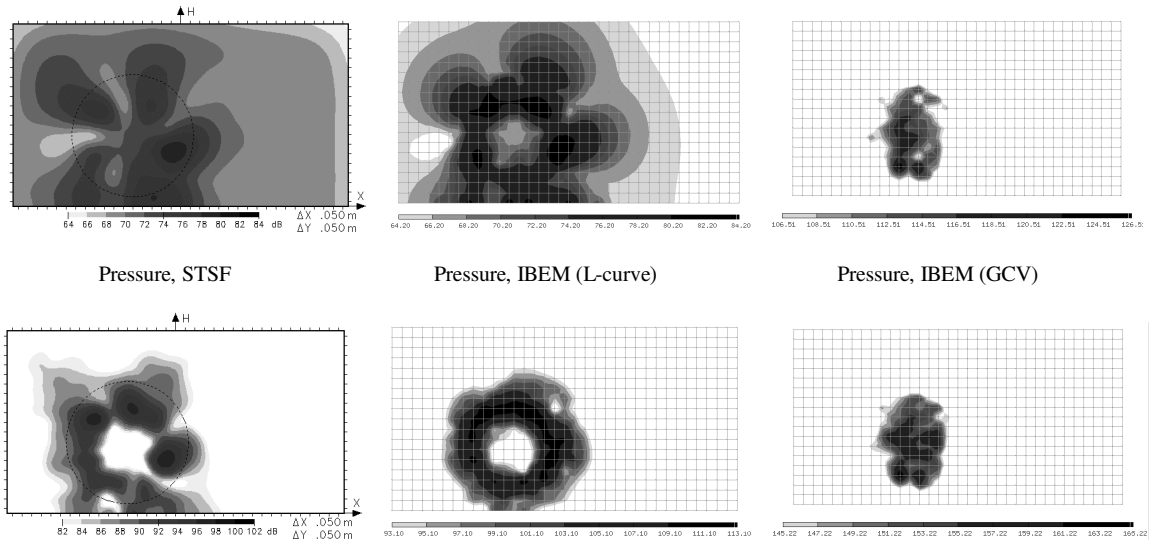

Pressure, STSF | Pressure, IBEM (L-curve) | Pressure, IBEM (GCV)

Particle velocity, STSF | Particle velocity, IBEM (L-curve) | Particle velocity, IBEM (GCV)